



This is a repository copy of *Chronic TNF α -driven injury delays cell migration to villi in the intestinal epithelium.*

White Rose Research Online URL for this paper:
<http://eprints.whiterose.ac.uk/135056/>

Version: Accepted Version

Article:

Muraro, D. orcid.org/0000-0001-9601-237X, Parker, A., Vaux, L. et al. (7 more authors) (2018) Chronic TNF α -driven injury delays cell migration to villi in the intestinal epithelium. *Interface*, 15 (145). 20180037. ISSN 1742-5689

<https://doi.org/10.1098/rsif.2018.0037>

© 2018 The Author(s). This is an author produced version of a paper subsequently published in *Interface*. Uploaded in accordance with the publisher's self-archiving policy.

Reuse

Items deposited in White Rose Research Online are protected by copyright, with all rights reserved unless indicated otherwise. They may be downloaded and/or printed for private study, or other acts as permitted by national copyright laws. The publisher or other rights holders may allow further reproduction and re-use of the full text version. This is indicated by the licence information on the White Rose Research Online record for the item.

Takedown

If you consider content in White Rose Research Online to be in breach of UK law, please notify us by emailing eprints@whiterose.ac.uk including the URL of the record and the reason for the withdrawal request.



eprints@whiterose.ac.uk
<https://eprints.whiterose.ac.uk/>

**Chronic TNF α -driven injury delays cell migration to villi in
the intestinal epithelium**

Journal:	<i>Journal of the Royal Society Interface</i>
Manuscript ID	rsif-2018-0037.R2
Article Type:	Research
Date Submitted by the Author:	n/a
Complete List of Authors:	Muraro, Daniele; Wellcome Trust Sanger Institute, ; University of Oxford, Mathematical Institute Parker, Aimee; Institute of Food Research Vaux, Laura; Institute of Food Research Filippi, Sarah; Imperial College London Almet, Axel; University of Oxford, Mathematical Institute Fletcher, Alexander; University of Sheffield, School of Mathematics and Statistics; University of Sheffield, Bateson Centre Watson, Alastair; University of East Anglia, Norwich Medical School Pin, Carmen; Institute of Food Research Maini, Philip; University of Oxford, Mathematics Byrne, Helen; University of Oxford,
Categories:	Life Sciences - Mathematics interface
Subject:	Biomathematics < CROSS-DISCIPLINARY SCIENCES, Computational biology < CROSS-DISCIPLINARY SCIENCES, Systems biology < CROSS-DISCIPLINARY SCIENCES
Keywords:	intestinal crypts, cell migration, cell-based model, compartmental model

Chronic $\text{TNF}\alpha$ -driven injury delays cell migration to villi in the intestinal epithelium

Daniele Muraro^{1,2,*}, Aimee Parker³, Laura Vaux³, Sarah Filippi⁴, Axel A. Almet¹, Alexander G. Fletcher⁵, Alastair J. M. Watson⁶, Carmen Pin³, Philip K. Maini¹, Helen M. Byrne¹

1 Wolfson Centre for Mathematical Biology, Mathematical Institute, University of Oxford, Oxford, United Kingdom

2 Wellcome Trust Sanger Institute, Wellcome Trust Genome Campus, Hinxton, Cambridgeshire, United Kingdom

3 Gut Health and Food Safety Research Programme, Institute of Food Research, Norwich, United Kingdom

4 Department of Mathematics, Department of Epidemiology and Biostatistics, Imperial College London, London, United Kingdom

5 School of Mathematics and Statistics and Bateson Centre, University of Sheffield, Sheffield, United Kingdom

6 Norwich Medical School, University of East Anglia, Norwich, United Kingdom

Abstract

The intestinal epithelium is a single layer of cells which provides the first line of defence of the intestinal mucosa to bacterial infection. Cohesion of this physical barrier is supported by renewal of epithelial stem cells, residing in invaginations called crypts, and by crypt cell migration onto protrusions called villi; dysregulation of such mechanisms may render the gut susceptible to chronic inflammation. The impact that excessive or misplaced epithelial cell death may have on villus cell migration is currently unknown. We integrated cell-tracking methods with computational models to determine how epithelial homeostasis is affected by acute and chronic $\text{TNF}\alpha$ -driven epithelial cell death. Parameter inference reveals that acute inflammatory cell death has a transient effect on epithelial cell dynamics, whereas cell death caused by chronic elevated $\text{TNF}\alpha$ causes a delay in the accumulation of labelled cells onto the villus compared to control. Such a delay may be reproduced by using a cell-based model to simulate the dynamics of each cell in a crypt-villus geometry, showing that a prolonged increase in cell death slows the migration of

*To whom correspondence should be addressed: Daniele.Muraro@sanger.ac.uk

1
2
3
4
5
6
7
8
9
10
11
12 cells from the crypt to the villus. This investigation highlights which injuries (acute or chronic) may be
13 regenerated and which cause disruption of healthy epithelial homeostasis.

14 Introduction

15 The intestinal epithelium is a rapidly self-renewing tissue, formed of a single layer of cells, that covers the
16 luminal surface of the small and large intestine, providing a barrier to bacterial infection. Epithelial cells
17 in the small intestine are organised into numerous protrusions, termed villi, and invaginations, termed
18 crypts of Lieberkühn. Self-renewal is sustained by the proliferative activity of adult stem cells at the
19 base of intestinal crypts whose progeny proliferate and then differentiate into the functionally distinct
20 epithelial subtypes that migrate onto the villus where they are eventually shed into the gut lumen [1].
21 Such cellular dynamics can be thought of as a ‘conveyor belt’ where cell proliferation acts as the principal
22 driving force for cell migration on villi [2]. Perturbations of this tightly controlled process may be
23 responsible for the development of serious diseases. For example, excessive or misplaced cell death may
24 disrupt barrier function and cause chronic inflammation; on the other hand, deficiency in cell death may
25 lead to cancer development [3]. In combination with experimental studies, mathematical modelling helps
26 us to disentangle the complex interactions underlying the self-renewal of the intestinal epithelium under
27 healthy and pathological conditions. The cellular dynamics of the intestinal epithelium have been studied
28 using a variety of theoretical approaches, including compartmental models based on ordinary differential
29 equations (ODEs) [4], [5], continuum models [6], cell-based models [7], [8], [9] - [17]. Experimental and
30 theoretical studies of the influence of reduced or halted proliferation on epithelial homeostasis showed
31 a pronounced coupling of cell proliferation with cell migration onto villi [18], [2]. However, it remains
32 unknown whether an increase in cell death in the epithelium affects villus cell migration and how excessive
33 cell death on a particular villus influences epithelial homeostasis in neighbouring crypts.

34 Here, we use a multidisciplinary approach to determine how two types of induced enterocyte cell
35 death affect cell migration on villi in two regions of the mouse small intestine (ileum and duodenum).
36 **Epithelial** cell death was induced by exposure to $\text{TNF}\alpha$, a cytokine involved in systemic inflammation,
37 for different time periods and levels. $\text{TNF}\alpha$ is well documented as an initiating agent in mouse models of
38 inflammatory bowel disease and has previously been used to study chronic inflammatory processes of the
39 intestine [19] - [24]. **However, we recognise that intestinal inflammation involves a multitude of cytokine**

1
2
3
4
5
6
7
8
9
10
11
12
13
14
15
16
17
18
19
20
21
22
23
24
25
26
27
28
29
30
31
32
33
34
35
36
37
38
39
40
41
42
43
44
45
46
47
48
49
50
51
52
53
54
55
56
57
58
59
60

and cellular responses, many of which may not be recapitulated in our TNF-only models, which may more strictly be described as TNF α -driven models of increased epithelial cell death, or more simply acute and chronic ‘injury’. During ‘acute injury’ the mice expressed a high level of circulating TNF α for around 90 minutes before levels returned to baseline; this treatment caused cleaved-Caspase-3 positive (apoptotic) cell death and detachment from villus tips. During ‘chronic injury’ the mice expressed a lower circulating level of TNF α for two weeks continuously prior to and during the measurements; this treatment induced less severe, but more persistent, cell death.

To investigate epithelial cell dynamics during acute and chronic injury, we applied cell-tracking methods to monitor accumulation of labelled cells along the crypt-villus axis following exposure of healthy crypts to high and low doses of TNF α . We generated experimental time courses from crypt-villus epithelial units (CVEU) indicating the number of cells that were tracked (labelled) in the crypt and villus compartments. A previous analysis of the kinetics of villus cell populations in mice involved deriving a median villus transit time [25]. Although this measurement may provide interesting information about the villus kinetics, the scope of our article is to quantify the contribution to migration in time from the crypt and to estimate how such contribution may be affected by cell death due to TNF α . For this reason, we developed mathematical models describing the dynamics along the crypt-villus unit which couple the effects of cell proliferation, migration and death. Complementary information was derived from two different computational approaches, namely cell-based and compartmental models, as follows. We replicated the experiments, simulating injury in a cell-based model in which cells are confined to a 2D surface comprising four crypts, adjacent to a villus, with cells moving according to a nearest-neighbour-defined repulsive force [15]. This model allows us to describe the spatial dynamics of cells on a crypt-villus geometry and to generate simulated time-courses that can be compared to the experimental time courses via time-dependent compartmental models as described below; however, the parameters of the cell-based model cannot be easily inferred from the experimental data since fitting such a detailed and stochastic model would be computationally intensive. By contrast, the compartmental models are described by a smaller number of parameters, since they do not account for the parameters associated with the crypt-villus geometry, and their simulation is computationally inexpensive. These advantages come at the expense of the biological detail included in the model: it accounts only for the time evolution of the number of cells in the crypt and villus compartments and neglects spatial effects. A schematic of our approach is presented in Figure 1. As in Parker et al [2], we first developed a compartmental model

1
2
3
4
5
6
7
8
9
10
11
12
13
14
15
16
17
18
19
20
21
22
23
24
25
26
27
28
29
30
31
32
33
34
35
36
37
38
39
40
41
42
43
44
45
46
47
48
49
50
51
52
53
54
55
56
57
58
59
60

69 that distinguishes two compartments, crypt and villus, and obtained quantitative estimates of parameters
70 describing cell proliferation, migration and death by fitting it to the experimental data using a variant of
71 Hamiltonian Monte Carlo (the No-U-Turn sampler) [26]. The posterior predictive distributions, showing
72 the simulated time evolution of the number of labelled cells in the crypts and in the villi, produced fits
73 that are in good agreement with the trend of the experimental time courses and highlighted that chronic
74 **elevated $TNF\alpha$** caused an increase in cell death, which, in turn, generated a decrease in the accumulation
75 of labelled cells on villi. By contrast, acute **elevated $TNF\alpha$** generated a similar, but small, delay. The two-
76 compartment model relies on the simplifying assumption that all cells in the crypts proliferate, whereas
77 in practice only some of them do. For this purpose, we extended the two-compartment model by includ-
78 ing a further compartment which enables us to distinguish between proliferative and non-proliferative
79 crypt cells. As for the two-compartment model, the three-compartment model produced fits that are
80 in good agreement with the experimental time courses; in addition, it generated predictions about the
81 dynamics of the number of proliferative and non-proliferative cells in the crypt. To investigate how an
82 increase in cell death may influence an accumulation of labelled cells from the crypt to the villus, we
83 then used the cell-based model to simulate injury due to treatments causing acute and chronic **epithelial**
84 **cell death**. Quantitative estimates of the parameters of the compartmental models, derived by model
85 fitting against these synthetic time courses, revealed a decrease in the accumulation of labelled cells on
86 villi under chronic injury and a minor decrease under acute injury, as experimentally observed. **Our**
87 **cell-based simulations account for multiple crypts and they qualitatively agree with the compartmental**
88 **models describing an average crypt-villus unit when comparing injuries against controls. This agreement**
89 **and the increase in the number of parameters in compartmental models accounting for multiple crypts**
90 **and villi, making their parameter values poorly identifiable (see for example [27]), supports our simplifi-**
91 **cation of analysing average crypt-villus units.** The consensus between the compartmental and cell-based
92 models also suggests that injuries caused by acute and chronic **elevated $TNF\alpha$** manifest themselves via
93 treatment-specific decreases in the accumulation of labelled cells on villi.

Methods

Experimental data

Animals

All animal experiments were conducted in strict accordance with the Home Office Animals (Scientific Procedures) Act 1986. Female C57BL/6 mice, aged 10-12 weeks and weighing at least 20 g prior to use in experiments, were housed and maintained in SPF conditions at the University of East Anglia, Norwich, UK in accordance with HO regulations, and all procedures were performed by fully-trained and licenced researchers. Experimental animals were closely monitored and were sacrificed by rising CO₂ and cervical dislocation, at the timepoints described in the text, prior to subsequent tissue collection. All animals were regularly monitored for clinical signs, any displaying signs beyond those expected within the moderate limits of the procedures would be immediately sacrificed by the above methods and not included in experimental data.

Induction of **enterocyte death**, cell labelling and tissue processing

Transient, acute **elevated circulating TNF α** was induced by single intraperitoneal injection of recombinant murine TNF α (Peprotech, London, UK) at 0.5 mg/kg. Chronic **elevated circulating TNF α** was achieved by hydrodynamic tail vein delivery of TNF α -expressing plasmid (originally a kind gift from C. Gunther, Erlangen, Germany). TNF α overexpression was confirmed by specific ELISA (Thermo Fisher Scientific, Waltham, USA) for elevated levels in blood plasma over a minimum of 14 days, and in liver and intestinal tissue lysates post mortem. The thymine analogue 5-bromo-2-deoxyuridine, BrdU, (Sigma-Aldrich, Paisley, UK) was administered at 50 mg/kg body weight by single intraperitoneal injection. In the case of acute **elevated TNF α** , BrdU was delivered simultaneously with TNF α . In the chronic **TNF** experiments, BrdU time-courses were performed once elevated blood TNF α levels had been established. At time points from 1h - 48h post BrdU-administration, mice were euthanised and intestinal tracts were removed, dissected, formalin-fixed and paraffin embedded. Transverse sections of duodenum and ileum were prepared at 5 μ m and were immunostained for BrdU using biotinylated anti-BrdU antibody (Ab-Cam, Cambridge, UK), Neutravidin-HRP (Thermo Fisher), and diaminobenzidine reaction (DAB, Dako, Glostrup, Denmark). Villus cell shedding was confirmed histologically by Caspase-3 (anti-CC3, R&D Systems, Minneapolis, USA) labelling of apoptotic cells in FFPE duodenal and ileal sections counterstained

1
2
3
4
5
6 with H&E.
7

8 9 **Data collection**

10
11 Collection of the experimental dataset followed the format described in Parker et al [2]. Although many
12 crypts contribute to a single villus, our experimental data and analysis describe single crypt-villus epithe-
13 lial units, i.e., a single continuous strip of epithelial cells running from the base of a particular crypt to
14 the tip of the associated villus, all within the same single strip of contiguous epithelial cells. The number
15 of unlabelled and BrdU-labelled cells by position, from crypt base to neighbouring villus tip, was counted
16 for 30-50 individual crypt-villus units per section, per region, per mouse to provide a good estimate of
17 the average behaviour of any individual strip in vivo (average crypt-villus epithelial units). Counts were
18 recorded as binary values; this generated, for each replicate and at each time point, a binary vector whose
19 length varied with the particular sample. Counts were taken at multiple time-points post-delivery of BrdU
20 and post delivery of TNF α (examples of histology and staining are shown in Supplementary Figure 1).
21 The counts and the code to calculate the experimental time courses are reported in the Supplementary
22 Data (folder Counts at <https://tinyurl.com/y9xk3nsk>). The number of samples for each time point
23 are shown in Supplementary Tables 1 and 2. The boundary between the crypt and villus compartment
24 was estimated from all datasets obtained during the first 2 hours after BrdU injection as the cell position
25 closest to the crypt bottom and such that the fraction of labelled cells in the villus is smaller than 0.01.
26 The time courses obtained from the ileum are presented in Figure 2a; the corresponding time courses
27 from the duodenum are presented in Figure 2b.
28
29
30
31
32
33
34
35
36
37
38
39
40

41 **Compartment-based models**

42
43 To analyse the spatio-temporal dynamics of BrdU-labelled cells we derived two compartmental models
44 formulated as a system of time-dependent ordinary differential equations (ODEs). The first model treats
45 the crypt-villus unit as two distinct compartments and distinguishes the cell numbers in the crypt and
46 villus; the second model decomposes the crypt-villus unit into three compartments and distinguishes
47 between proliferative and non-proliferative cells in the crypt. For simplicity, and to allow for parameter
48 estimation, in what follows we model labelled cells only.
49
50
51
52
53
54
55
56
57
58
59
60

Two-compartment model

We distinguish two cellular compartments: labelled cells in the crypt, whose number at time t is denoted by $C = C(t)$, and labelled cells in the villus, whose number is denoted by $V = V(t)$. We introduce two parameter thresholds C^*, V^* such that when $C(t) > C^*$ labelled cells in the crypt start migrating onto the villus, and when $V(t) > V^*$ cells begin to be shed from the villus. We denote condition-specific death rates in the crypt and villus compartment as follows:

$$\mu_c^{(\text{condition})} = \begin{cases} 0 & \text{in control (BrdU)} \\ \mu_{c_a} & \text{during acute injury} \\ \mu_{c_c} & \text{during chronic injury} \end{cases} \quad \mu_v^{(\text{condition})} = \begin{cases} 0 & \text{in control (BrdU)} \\ \mu_{v_a} & \text{during acute injury} \\ \mu_{v_c} & \text{during chronic injury} \end{cases} \quad (1)$$

where $\mu_{c_a}, \mu_{c_c}, \mu_{v_a}, \mu_{v_c}$ are positive constants. Defining by

$$H(x) = \begin{cases} 0 & \text{if } x < 0 \\ 1 & \text{if } x \geq 0, \end{cases}$$

the Heaviside function, the two-compartment model is described by the following pair of ODEs:

$$\begin{aligned} \frac{dC}{dt} &= \lambda C - \gamma(C - C^*)H(C - C^*) - \mu_c^{(\text{condition})}C \\ \frac{dV}{dt} &= \gamma(C - C^*)H(C - C^*) - \gamma_s(V - V^*)H(V - V^*) - \mu_v^{(\text{condition})}V \end{aligned} \quad (2)$$

where λ is the net cell proliferation rate (cell proliferation minus cell death rate), γ is the cell migration rate between the two compartments, γ_s is the cell shedding rate from the villus. Model parameters and initial conditions, included in the set of parameters to be estimated, are listed in Table 1.

Three-compartment model

The three-compartment model subdivides the crypt into proliferative and non-proliferative cells and defines the following compartments: labelled proliferative cells in the crypt, whose number at time t is denoted by $P = P(t)$; labelled non-proliferative cells in the crypt, whose number is denoted by $Q = Q(t)$ and labelled non-proliferative cells on the villus, whose number is denoted by $V = V(t)$ (cells on the villus do not proliferate). For comparison with the two compartment model, we also denote

by $C(t) = P(t) + Q(t)$ the total number of labelled cells in the crypt. We introduce three parameter thresholds P^*, Q^*, V^* such that when $P(t) > P^*$ labelled proliferative cells start migrating onto the villus, when $Q(t) > Q^*$ non-proliferative labelled cells start migrating onto the villus and when $V(t) > V^*$ cell shedding begins to occur from the villus. As we set up the crypt-villus boundary at the cell position closest to the crypt bottom where we detected proliferative cells, we deemed both proliferative and non-proliferative cells as likely to pass this threshold and to be transferred to the non-proliferative villus compartment. Alternatively other boundaries (such as the crypt mouth) between crypt and villus could be considered. Depending on where the boundary is located one could argue that only non-proliferative cells are transferred onto the villus or that the rates of transfer are not equal for proliferative and non-proliferative cells. In what follows, we assume that both proliferative and non-proliferative cells can migrate onto villi and may be affected by acute and chronic **injury**; for simplicity, we assume equal rates of cell transfer onto villi and of cell death in the crypts. We denote condition specific death rates in the crypt and villus compartments as for the two-compartment model (see Equations (1)). The three-compartment model is described by the following system of time-dependent ODEs:

$$\begin{aligned}
 \frac{dP}{dt} &= (\lambda - \gamma_c)P - \gamma_v(P - P^*)H(P - P^*) - \mu_c^{(\text{condition})}P \\
 \frac{dQ}{dt} &= \gamma_cP - \gamma_v(Q - Q^*)H(Q - Q^*) - \mu_c^{(\text{condition})}Q \\
 \frac{dV}{dt} &= \gamma_v(P - P^*)H(P - P^*) + \gamma_v(Q - Q^*)H(Q - Q^*) - \gamma_s(V - V^*)H(V - V^*) - \mu_v^{(\text{condition})}V
 \end{aligned} \quad (3)$$

where λ is the cell net proliferation rate, γ_c is the rate at which cells differentiate from a proliferative to a non-proliferative state, γ_v is the rate at which cells migrate onto the villus, γ_s is the rate of cell shedding from the villus and H is the Heaviside function. Model parameters and initial conditions, included in the set of parameters to be estimated, are listed in Table 2.

Cell-based simulations

We simulated injury by using a cell-based simulation of cell dynamics on a patch of intestinal epithelium composed of multiple crypts and a single villus, previously developed by Mirams et al. [15], and generated synthetic time courses.

The model is a stochastic 3D off-lattice cell centre based model confined to a 2D surface comprising four crypts that surround a single villus; the crypts and the villus are modelled using a cylindrical

1
2
3
4
5
6 geometry with spherical rims. Cell movement is driven by a nearest-neighbour-defined force, previously
7 employed by Meineke et al. [9]. Each pair of neighbouring nodes is assumed to be connected by a linear
8 spring. The force of node i is given by
9

$$10 \quad \mathbf{F}_i(t) = \sum_j \mu_{i,j} (|\mathbf{r}_{i,j}| - s_{i,j}(t)) \hat{\mathbf{r}}_{i,j},$$

11
12
13
14
15
16 where $\mu_{i,j}$ is the spring constant for the spring between nodes i and j , $s_{i,j}(t)$ is its natural length at
17 time t , $\mathbf{r}_{i,j}$ is their relative displacement and a hat ($\hat{\cdot}$) denotes a unit vector. Cells moving above a
18 plane defined at the villus tip are removed due to anoikis. Injury is simulated either by removing cells
19 randomly (during chronic injury) or by initially removing cells that are above a plane defined at $\frac{2}{3}$ of
20 the villus height (to account for the experimentally observed detachment of cells at the top third of
21 the villus during acute injury). Cell proliferation depends on a decreasing gradient of the Wnt family
22 of morphogens from the crypt to the villus [30] and it is modelled by defining a linear gradient in Wnt
23 concentration up the crypt, allowing cells to divide when their Wnt concentration exceeds a fixed threshold
24 (see SimpleWntCellCycleModel class for details [15]).
25
26
27
28
29
30

31 All simulations were initialised without including any random removal of cells and were run for 1000
32 h with default parameter values [15], at which time the total number of cells in the crypts and in the
33 villus was approximately constant. After initialisation, cell-based simulations at homeostasis (control)
34 were run for 80 hours with default parameter values. During this time period, crypt cells were labelled
35 and their lineage was tracked according to their ancestor proliferative cell. Acute injury was modelled by
36 initially detaching cells from the top third of the villus. Regeneration of this area, due to cell migration
37 from the crypts, was simulated for 80 hours. Chronic injury was introduced by randomly killing cells in
38 the crypts and the villus with the default probability value $p = 0.005 h^{-1}$.
39
40
41
42
43
44

45 Parameter estimation

46
47
48 The compartmental models were solved using the R-packages deSolve (Classical Runge-Kutta 4th Order
49 Integration) [29] and RSTAN [26]. STAN is a C++ library that performs Bayesian inferences using the
50 No-U-Turn sampler (a variant of Hamiltonian Monte Carlo); the RSTAN package conveniently allows
51 STAN to be used from R. RSTAN was applied to Equations (2) and (3) with uniform priors represented
52 in Supplementary Figures 14, 16, 18, 20, 22, 24. Convergence diagnostics were then calculated for four
53
54
55
56
57
58
59
60

1
2
3
4
5
6
7 174 Markov Chain Monte Carlo (MCMC) chains using the R package CODA, which provides routines for
8 175 output analysis and diagnostics for MCMC [31]. Where multi-modality was highlighted by chains mixing
9 176 around different modes, the chains with the highest fit quality (STAN log probability variable lp_) were
10 177 selected. The initial conditions for $P(t)$, $Q(t)$ (three-compartment model) and $C(t)$ (two-compartment
11 178 model) were included in the set of parameters to be estimated by applying MCMC. Since the number of
12 179 labelled cells in the villus ($V(t)$) is approximately zero at the start of the time courses, we assumed that
13 180 migration of labelled cells onto villi may be initially neglected.

20 Results

21
22 181 In what follows, we first describe the predictions of our compartmental and cell-based models regarding
23 182 the influence of elevated $\text{TNF}\alpha$ on epithelial homeostasis; we then discuss the parameters inferred when
24 183 fitting the compartmental models to experimental and simulated data.

25
26
27
28 184 **Accumulation of labelled cells on villi is delayed during chronic epithelial damage.** The two-
29 185 and three-compartment models were fitted against the experimental data derived from the ileum and the
30 186 duodenum as described in the Methods section. The resulting posterior predictive distributions are shown
31 187 in Figures 3, 4 and Supplementary Figures 3, 4. Both models reproduce the trend of the experimental data
32 188 and show a delay in migration during chronic injury compared to control (see Figure 5 and Supplementary
33 189 Figure 5). Acute epithelial damage causes a modest delay in cell migration terms in the ileum and a very
34 190 small decrease in the duodenum (Figure 5 and Supplementary Figure 5). These findings may appear
35 191 counterintuitive, since some inflammatory conditions are associated with crypt enlargement. However,
36 192 we did not observe epithelial hyperproliferation or increased crypt size in our TNF-driven damage model.
37 193 In fact the number of crypt cells was slightly reduced, likely due to increased cell death during damage.

38
39
40
41
42
43
44 194 The parameter posterior distributions obtained in the duodenum compared to the ileum highlight
45 195 higher cell proliferation rates (see Supplementary Figures 9 and 10) leading to higher values of the
46 196 migration terms (see Figure 5 and Supplementary Figure 5). Although it is currently unknown why
47 197 the proliferation rates are differing in the duodenum, they likely reflect local stem cell responses to the
48 198 differencing microbial, immunological and metabolic cues..

1
2
3
4
5
6
7 **199 Cell-based simulations suggest that injuries drive treatment specific delays in cell migration.**
8
9
10
11
12
13
14
15
16
17
18
19
20
21
22
23
24
25
26
27
28
29
30
31
32
33
34
35
36
37
38
39
40
41
42
43
44
45
46
47
48
49
50
51
52
53
54
55
56
57
58
59
60

200 The cell-based model was simulated as described in the Methods section ‘Cell-based simulations’. Typical
201 simulation results are presented in the Supplementary Data (file Cell_Based_Simulations.pptx at [https://](https://tinyurl.com/y9xk3nsk)
202 tinyurl.com/y9xk3nsk). Supplementary Figure 2 shows the mean and standard errors of simulated time
203 series of labelled cells generated by ten simulations for each condition. Compared to control simulations,
204 the simulated persistent, increased rate of cell death associated with chronic injury appears to hinder
205 the migration of labelled crypt cells onto the villus. Conversely, the initial detachment of cells from the
206 villus tip caused by simulated acute injury does not seem to affect significantly cell migration from the
207 crypts to the villus and the villus tip regenerates due to cell migration from the crypts. To confirm
208 these effects, we then fitted the compartmental models to the time courses generated from simulations
209 of the cell-based model. The simulated data were fitted up to 50 hours to emulate the duration of the
210 experimental time courses. Supplementary Figures 6 and 7 show the posterior predictive distributions of
211 the two- and three-compartment models together with the predicted migration terms. As observed when
212 applying the model to the experimental data, an increase in cell death caused a delay in the accumulation
213 of labelled cells on villi during simulated chronic **injury** and a minor delay due to simulated acute **injury**
214 (Supplementary Figure 8). The posterior distributions of the parameter are presented in Supplementary
215 Figures 9-24. A prolonged delay in the accumulation of labelled cells on villi during chronic **injury**
216 compared to acute **injury** is caused by the combined increase in the death rates in the crypts (μ_c) and
217 in the villi (μ_v), (Supplementary Figures 9-12). We finally analysed the influence of the geometry of
218 the setup chosen for the cell-based simulations on the migration terms by simulating time courses when
219 varying crypt and villus lengths and radii. These time courses were fitted using the two-compartment
220 model and the migration terms were derived from the fitted model. The results are discussed in the
221 section “Influence of the geometry of the setup chosen for the cell-based simulations on the migration
222 terms” in the Supplementary Material. Whereas an increase in villus length or radius plays a minor role
223 on the migration term, an increase in crypt length or radius causes faster cell migration onto the villus
224 (see Supplementary Figure 33, 34, 35).

225 **Small regions of the parameter search space allow for good quality fits.** Highly correlated
226 parameters may be found in both of the compartment models. In particular, the pairs (λ, μ_{c_c}) and
227 (γ, C^*) are the most strongly correlated parameters in the two-compartment model in both tissues

(Supplementary Figures 13 and 15); whereas, (λ, γ_c) , (λ, P^*) , (γ_c, P^*) , (λ, P_0) , (P^*, P^0) , (P_0, Q_0) are the most correlated pairs in the three-compartment model in both tissues (Supplementary Figures 17 and 19). Highly correlated pairs were also found when fitting the compartment models against simulated data; for example, (λ, C_0) , (γ, C^*) , (λ, γ_s) in the two-compartment model (Supplementary Figure 21) and (λ, γ_c) , (λ, P^*) , (γ_c, P^*) , (λ, P_0) , (P^*, P^0) , (P_0, Q_0) and others in the three-compartment model (Supplementary Figure 23). Notwithstanding this dependence between different parameters, density plots of the posterior distributions highlight that relatively small regions of the parameter search space, defined by uniform prior distributions, allow for good quality fits (Supplementary Figures 14, 16, 18, 20, 22, 24).

The time thresholds associated with cell migration and cell shedding are most sensitive to crypt parameters. Because of the increase of the death rates μ_c and μ_v during acute and chronic injury, we analysed how changes in these parameters in the two-compartment model may affect the time thresholds above which cell migration and cell shedding begin. More precisely, we denoted by t_C^* and t_V^* the time thresholds after which $C(t) > C^*$ and $V(t) > V^*$, respectively. Simulation of the perturbed model highlighted that increasing μ_c causes a delay in both time thresholds, whereas μ_v only affects t_V^* (Supplementary Figure 25). Supplementary Figures 26 - 28 show how the time thresholds vary when all model parameters are varied and highlight that both thresholds are most sensitive to λ , μ_c and C_0 . Similar effects were found when simulating the three-compartment model by defining the thresholds t_P^* , t_Q^* , t_C^* and t_V^* , after which $P(t) > P^*$, $Q(t) > Q^*$, $C(t) := P(t) + Q(t) > P^* + Q^* =: C^*$ and $V(t) > V^*$, respectively. Simulation of the perturbed model highlighted that increasing μ_c causes all time thresholds (t_P^* , t_Q^* , t_C^* , t_V^*) to increase, whereas increasing μ_v causes an increase in t_V^* only (Supplementary Figure 29). Supplementary Figures 30 - 32 show how the time thresholds vary when all other model parameters vary and highlight that all of these thresholds are extremely sensitive to the values of λ , μ_c , γ_c and P_0 .

Discussion

By combining cell tracking methods with computational models we derived quantitative estimates of the proliferative activity of crypt stem cells and of their influence on villus cell migration during **TNF α -driven epithelial injury** conditions. Experimental time courses were analysed by fitting the data to compartmental models with two and three compartments. Both fitted models were able to reproduce well the trend of the experimental time courses. The three-compartment model allowed prediction of

1
2
3
4
5
6
7 255 the time evolution of proliferative and non-proliferative cells at the expense of requiring estimation of
8 256 a greater number of unknown parameter values when compared to the two-compartment model. The
9
10 257 posterior parameter and predictive distributions highlighted in both models that, whereas an acute and
11 258 temporary increase in cell death did not influence distinctly net cell proliferation (new born cells minus
12
13 259 dead cells) and migration onto the villus, a prolonged and less severe injury caused a decrease in net
14
15 260 cell proliferation which produced, in turn, a delayed migration. To further investigate how injury may
16
17 261 affect the dynamics of cells in the epithelium and trigger such delay, we simulated cell death, initiated
18 262 by $TNF\alpha$, by means of a cell-based model and generated simulated time courses. Analysis of these time
19
20 263 courses by means of compartmental models showed delayed migration under simulated chronic injury
21
22 264 as experimentally observed, highlighting how a prolonged increase in cell death affects the dynamics of
23
24 265 cells in the epithelium by delaying their migration. In summary, integration of computational modelling
25
26 266 with experimental data derived from cell tracking methods allowed us to distinguish which conditions
27
28 267 influence epithelial cell dynamics. Identification of such conditions may highlight their contribution
29
30 268 to barrier dysfunction in the development of intestinal inflammation. To the best of our knowledge, an
31
32 269 experimental and computational analysis of cell dynamics during villus injury such as the one described in
33
34 270 this article, which integrates compartmental and cell-based models with novel experimental time courses,
35
36 271 has not been presented before. We believe that this analysis may stimulate further experimental work to
37
38 272 estimate, for example, the proportion of proliferative and non-proliferative cells in the crypts.

38 Data accessibility

39
40
41 273 The datasets supporting this article have been uploaded as part of the electronic supplementary material.

44 Authors' contribution

45
46
47 274 D. Muraro and Axel A. Almet performed the computational analysis of the mathematical models; A.
48
49 275 Parker and L. Vaux designed and performed the experiments; S. Filippi contributed to implementing the
50
51 276 inference of the model parameters; A. G. Fletcher, P. K. Maini and H. M. Byrne contributed to designing
52
53 277 the work and developing the mathematical models; A. J. M. Watson participated in designing the work
54
55 278 and in experimental planning; C. Pin contributed to project design, mathematical model development,

1
2
3
4
5
6
7 279 experimental planning and data analysis. All of the authors contributed to writing the manuscript.
8
9

10 **Competing interests**

11
12 280 We declare we have no competing interests.
13
14

15 **Funding**

16
17
18 281 This work was funded by the Biotechnology and Biological Sciences Research Council (BBSRC)-UK
19
20 282 projects BB/K018256/1, BB/K017578/1, BB/K017144/1, and BB/J004529/1, by the Engineering and
21
22 283 Physical Sciences Research Council (EPSRC)-UK project EP/I017909 and by Cancer Research UK
23
24 284 (CRUK) grant number C5255/A23225, through a Cancer Research UK Oxford Centre Prize DPhil Stu-
25
26 285 dentship.
27

28 **Acknowledgements**

29
30
31 286 We thank Hunter Rice and the journal club on computational biology at the Department of Microbiology,
32
33 287 The University of Tennessee, Knoxville for helpful comments.
34
35
36
37
38
39
40
41
42
43
44
45
46
47
48
49
50
51
52
53
54
55
56
57
58
59
60

References

- [1] Watson AJM, Hughes KR. TNF α -induced intestinal epithelial cell shedding: implications for intestinal barrier function. *Annals of the New York Academy of Sciences*. 2012 Jun 25;1258(1):1-8. (doi:10.1111/j.1749-6632.2012.06523.x)
- [2] Parker A, Maclaren OJ, Fletcher AG, Muraro D, Kreuzaler PA, Byrne HM, et al. Cell proliferation within small intestinal crypts is the principal driving force for cell migration on villi. *The FASEB Journal*. 2016 Oct 20;31(2):636-49. (doi:10.1096/fj.201601002)
- [3] Becker C, Watson AJ, Neurath MF. Complex Roles of Caspases in the Pathogenesis of Inflammatory Bowel Disease. *Gastroenterology*. 2013 Feb;144(2):283-93. (doi:10.1053/j.gastro.2012.11.035)
- [4] Britton NF, Wright NA, Murray JD. A mathematical model for cell population kinetics in the intestine. *Journal of Theoretical Biology*. 1982 Oct;98(3):531-41. (doi:10.1016/0022-5193(82)90135-7)
- [5] Johnston MD, Edwards CM, Bodmer WF, Maini PK, Chapman SJ. Mathematical modeling of cell population dynamics in the colonic crypt and in colorectal cancer. *Proceedings of the National Academy of Sciences*. 2007 Feb 28;104(10):4008-13. (doi:10.1073/pnas.0611179104)
- [6] Murray PJ, Walter A, Fletcher AG, Edwards CM, Tindall MJ, Maini PK. Comparing a discrete and continuum model of the intestinal crypt. *Physical Biology*. 2011 Mar 16;8(2):26011. (doi:10.1088/1478-3975/8/2/026011)
- [7] Loeffler M, Stein R, Wichmann H-E, Potten CS, Kaur P, Chwalinski S. Intestinal Cell Proliferation. I. A Comprehensive Model of Steady-State Proliferation In the Crypt. *Cell Proliferation*. 1986 Nov;19(6):627-45. (doi:10.1111/j.1365-2184.1986.tb00763.x)
- [8] Loeffler M, Potten CS, Paulus U, Glatzer J, Chwalinski S. Intestinal Crypt Proliferation. II. Computer Modelling of Mitotic Index Data Provides Further Evidence For Lateral and Vertical Cell Migration In the Absence of Mitotic Activity. *Cell Proliferation*. 1988 Jul;21(4):247-58. (doi:10.1111/j.1365-2184.1988.tb00784.x)
- [9] Meineke FA, Potten CS, Loeffler M. Cell migration and organization in the intestinal crypt using a lattice-free model. *Cell Proliferation*. 2001 Aug;34(4):253-66. (doi:10.1046/j.0960-7722.2001.00216.x)

- 1
2
3
4
5
6
7
8
9
10
11
12
13
14
15
16
17
18
19
20
21
22
23
24
25
26
27
28
29
30
31
32
33
34
35
36
37
38
39
40
41
42
43
44
45
46
47
48
49
50
51
52
53
54
55
56
57
58
59
60
- 314 [10] van Leeuwen IMM, Mirams GR, Walter A, Fletcher A, Murray P, Osborne J, et al. An integrative
315 computational model for intestinal tissue renewal. *Cell Proliferation*. 2009 Oct;42(5):617-36. (doi:
316 10.1111/j.1365-2184.2009.00627.x)
- 317 [11] Mirams GR, Fletcher AG, Maini PK, Byrne HM. A theoretical investigation of the effect of prolif-
318 eration and adhesion on monoclonal conversion in the colonic crypt. *Journal of Theoretical Biology*.
319 2012 Nov;312:143-56. (doi:10.1016/j.jtbi.2012.08.002)
- 320 [12] Buske P, Galle J, Barker N, Aust G, Clevers H, Loeffler M. A Comprehensive Model of the Spatio-
321 Temporal Stem Cell and Tissue Organisation in the Intestinal Crypt. *PLoS Computational Biology*.
322 2011 Jan 6;7(1):e1001045. (doi:10.1371/journal.pcbi.1001045)
- 323 [13] Pin C, Watson AJM, Carding SR. Modelling the Spatio-Temporal Cell Dynamics Reveals Novel
324 Insights on Cell Differentiation and Proliferation in the Small Intestinal Crypt. *PLoS ONE*. 2012
325 May 18;7(5):e37115. (doi:10.1371/journal.pone.0037115)
- 326 [14] Dunn S-J, Näthke IS, Osborne JM. Computational Models Reveal a Passive Mechanism for Cell
327 Migration in the Crypt. *PLoS ONE*. 2013 Nov 18;8(11):e80516. (doi:10.1371/journal.pone.0080516)
- 328 [15] Mirams GR, Arthurs CJ, Bernabeu MO, Bordas R, Cooper J, Corrias A, et al. Chaste: An Open
329 Source C++ Library for Computational Physiology and Biology. *PLoS Computational Biology*. 2013
330 Mar 14;9(3):e1002970. (doi:10.1371/journal.pcbi.1002970) Code: [https://chaste.cs.ox.ac.uk/
331 trac/wiki/PaperTutorials/Plos2013/CryptsAndVillus](https://chaste.cs.ox.ac.uk/trac/wiki/PaperTutorials/Plos2013/CryptsAndVillus)
- 332 [16] Ingham-Dempster T, Walker DC, Corfe BM. An agent-based model of anoikis in the colon crypt dis-
333 plays novel emergent behaviour consistent with biological observations. *Royal Society Open Science*.
334 2017 Apr;4(4):160858. (doi:10.1098/rsos.160858)
- 335 [17] Ingham-Dempster T, Corfe B, Walker D. A cellular based model of the colon crypt suggests novel
336 effects for Apc phenotype in colorectal carcinogenesis. *Journal of Computational Science*. 2017 Jun.
337 (doi:10.1016/j.jocs.2017.06.013)
- 338 [18] Maclaren OJ, Parker A, Pin C, Carding SR, Watson AJM, Fletcher AG, et al. A hierarchical Bayesian
339 model for understanding the spatiotemporal dynamics of the intestinal epithelium. *PLOS Computa-
340 tional Biology*. 2017 Jul 28;13(7):e1005688. (doi:10.1371/journal.pcbi.1005688)

- 1
2
3
4
5
6
7 341 [19] Kontoyiannis D, Pasparakis M, Pizarro TT, Cominelli F, Kollias G. Impaired on/off regulation of
8 342 TNF biosynthesis in mice lacking TNF AU-rich elements: implications for joint and gut-associated
9 343 immunopathologies. *Immunity*. 1999 Mar; 10(3):387-98.
- 11
12 344 [20] Armaka M, Apostolaki M, Jacques P, Kontoyiannis DL, Elewaut D, Kollias G. Mesenchymal cell
13 345 targeting by TNF as a common pathogenic principle in chronic inflammatory joint and intestinal
14 346 diseases. *J Exp Med*. 2008; 205(2):331-7.
- 17
18 347 [21] Roulis M, Armaka M, Manoloukos M, Apostolaki M, Kollias G. Intestinal epithelial cells as producers
19 348 but not targets of chronic TNF suffice to cause murine Crohn-like pathology. *Proc Natl Acad Sci U*
20 349 *S A*. 2011 Mar 29;108(13):5396-401.
- 23
24 350 [22] Lau KS, Cortez-Retamozo V, Philips SR, Pittet MJ, Lauffenburger DA, Haigis KM. Multi-scale
25 351 in vivo systems analysis reveals the influence of immune cells on TNF- α -induced apoptosis in the
26 352 intestinal epithelium. *PLoS Biol*. 2012;10(9):e1001393
- 28
29 353 [23] Williams JM, Duckworth CA, Watson AJ, Frey MR, Miguel JC, Burkitt MD, Sutton R, Hughes KR,
30 354 Hall LJ, Caamao JH, Campbell BJ, Pritchard DM. A mouse model of pathological small intestinal
31 355 epithelial cell apoptosis and shedding induced by systemic administration of lipopolysaccharide. *Dis*
32 356 *Model Mech* 2013 (6):1388-99.
- 36
37 357 [24] Schaubeck M, Clavel T, Calasan J, Lagkouvardos I, Haange SB et al. Dysbiotic gut microbiota
38 358 causes transmissible Crohn's disease-like ileitis independent of failure in antimicrobial defence. *Gut*
39 359 2016;65(2):225-237. doi:10.1136/gutjnl-2015-309333.
- 41
42 360 [25] Wright NA, Irwin M. The kinetics of villus cell populations in the mouse small intestine. I. Normal
43 361 villi: the steady state requirement. *Cell Tissue Kinet*. 1982 Nov;15(6):595-609.
- 45
46 362 [26] The Stan Development Team Stan Modeling Language User's Guide and Reference Manual.
47 363 <http://mc-stan.org>
- 49
50 364 [27] Barthel ER. On the utility of a compartmental population kinetics model of intestinal epithelial stem
51 365 cell proliferation and differentiation *Theor Biol Med Model*. 2017; 14: 25.
- 53
54 366 [28] Barker N, van Es JH, Kuipers J, Kujala P, van den Born M, Cozijnsen M, et al. Identification of
55 367 stem cells in small intestine and colon by marker gene Lgr5. *Nature*. 2007;449(7165):1003-U1.

- 1
2
3
4
5
6
7 368 [29] Soetaert K, Petzoldt T, Setzer RW. Solving Differential Equations in R: Package deSolve. *Journal*
8 369 *of Statistical Software*. 2010;33(9). (doi:10.18637/jss.v033.i09)
9
10 [30] Gaspar C, Fodde R. APC dosage effects in tumorigenesis and stem cell differentiation. *The Interna-*
11 *tional Journal of Developmental Biology*. 2004;48(5-6):377-86. (doi:10.1387/ijdb.041807cg)
12 371
13
14 [31] Plummer M, Best N, Cowles K, Vines K. CODA: Convergence Diagnosis and Output Analysis for
15 372
16 373 MCMC. *R News*. 2006;6,7-11.
17
18
19
20
21
22
23
24
25
26
27
28
29
30
31
32
33
34
35
36
37
38
39
40
41
42
43
44
45
46
47
48
49
50
51
52
53
54
55
56
57
58
59
60

For Review Only

Main Figures

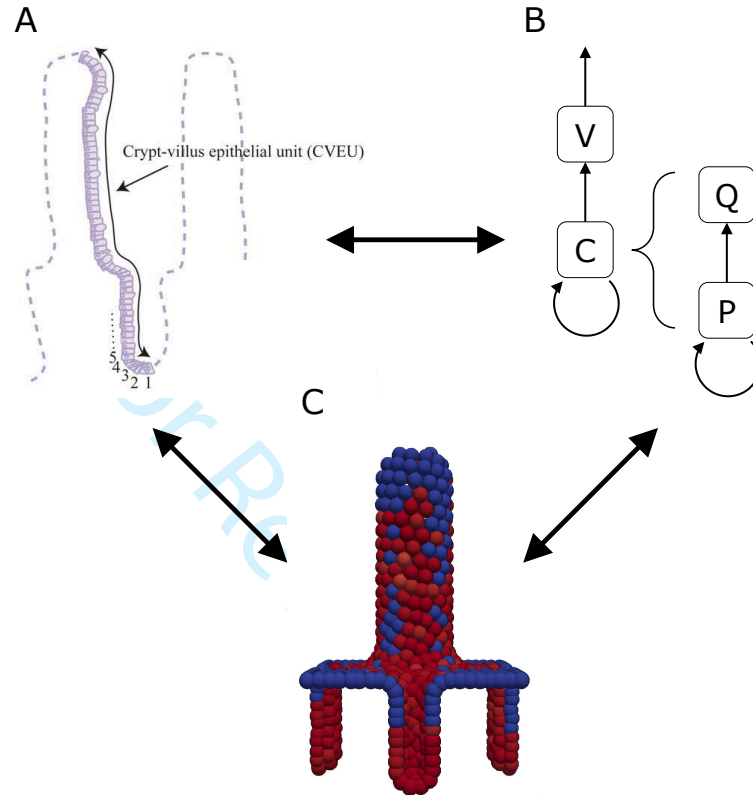


Figure 1: **Schematic of our approach.** A) Experimental time courses are derived from crypt-villus epithelial units (CVEU) and are analysed by counting labelled cells in the crypt and villus compartments. B) A compartment-based model accounting for crypt cells (C) and villus cells (V) allows us to quantify cell migration under injury and control. A model extension which distinguishes between a proliferative (P) and a non-proliferative (Q) compartment generates predictions on the dynamics of the number of proliferative and non-proliferative cells in the crypt. C) A multi-cellular model allows for replication of the experiment and for generation of simulated data; in red and blue are presented labelled and unlabelled cells, respectively. The arrows are interpreted as follows: A \rightarrow B (experimental data informing model parameterisation): The experimental data allow for inference of the compartment-based model parameters; B \rightarrow A (model prediction): The posterior predictive distributions highlight a decrease in the accumulation of labelled cells on villi which is specific of the type of injury (acute or chronic); A \rightarrow C (experimental background informing model development): The injuries caused by acute **elevated TNF α** (death and detachment of cells from villus tips) and chronic **elevated TNF α** (less severe, but more persistent, rates of cell death) inform the replication of the experiments (simulated injuries) by means of cell-based simulations and allow for generation of simulated time courses; B \leftrightarrow C (consensus between models): The posterior predictive distributions obtained when fitting the compartment based models to data simulated by means of the cell-based model highlight a qualitative agreement with the fits to the experimental data; C \rightarrow A (model prediction): The consensus between the models supports the driving role of the injuries caused by acute and chronic **elevated TNF α** in generating treatment specific decrease in the accumulation of labelled cells on villi.

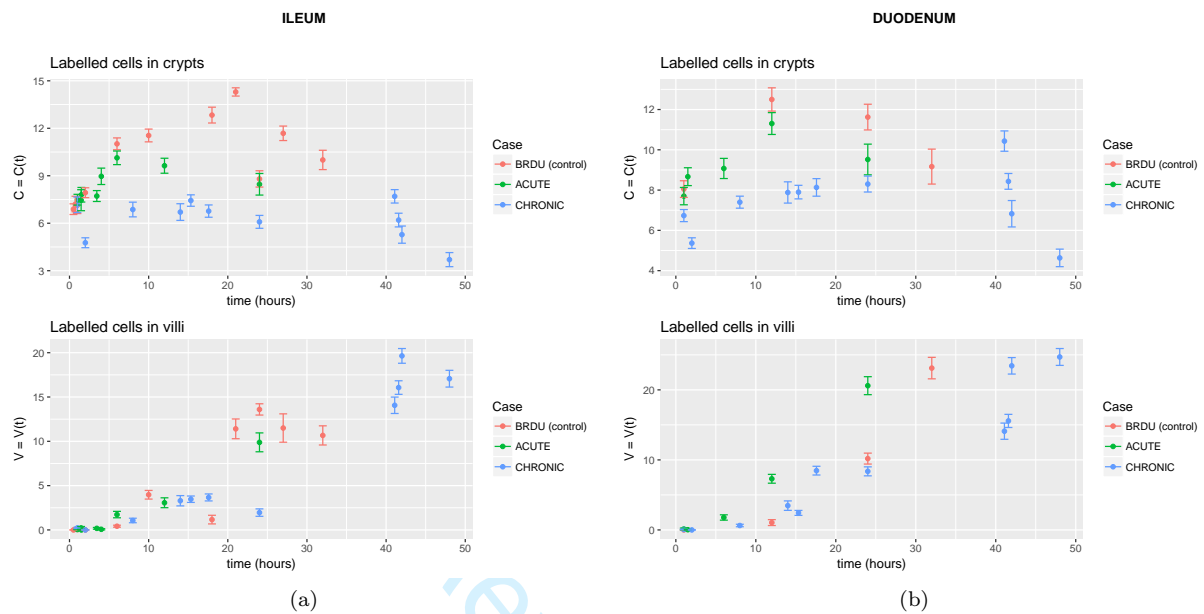


Figure 2: **Experimental data.** Time series representing average numbers of cells in crypts $C = C(t)$ and villi $V = V(t)$ during acute injury, chronic injury and control (BrdU) in ileum (a) and duodenum (b). Error bars indicate standard errors.

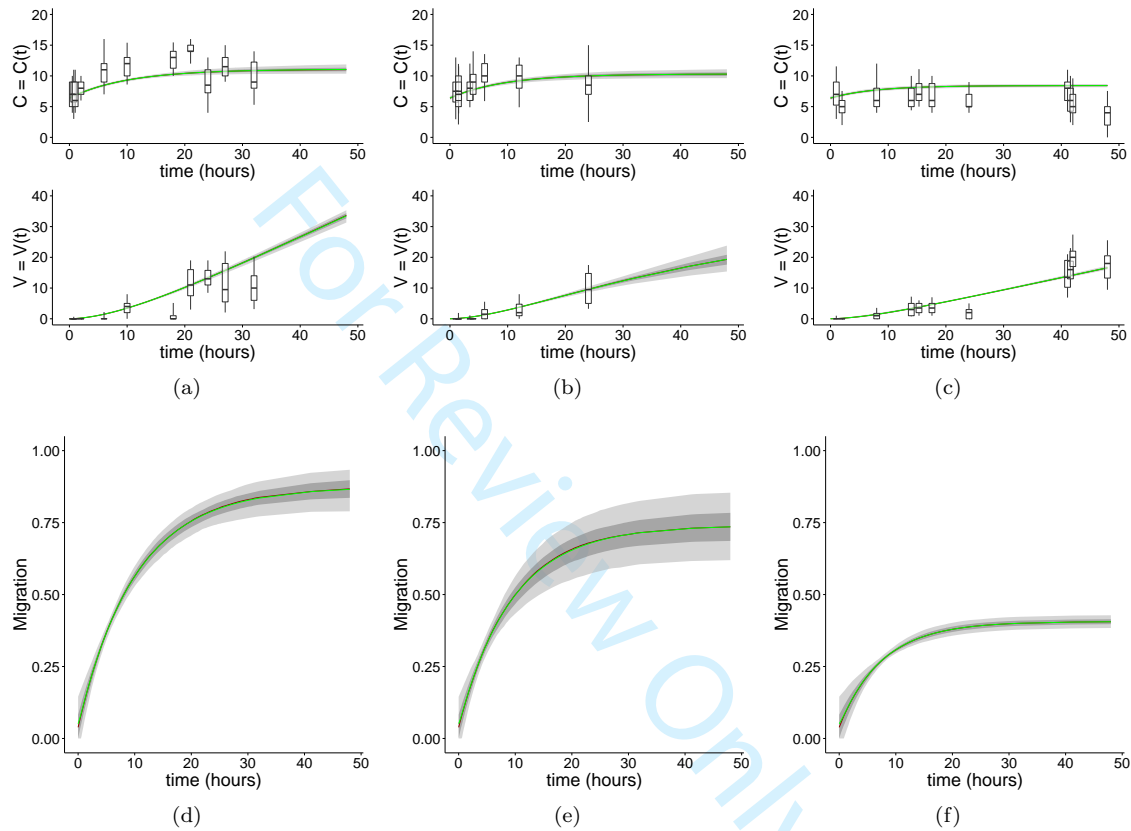


Figure 3: **Fits of the two-compartment model to ileal time course data.** (a)-(b)-(c) Posterior predictive distributions and estimates of parameter uncertainty obtained by fitting the two-compartment model (Eqs. (1)) against ileal time courses. Posterior predictive distributions inferred from (a) **BrdU (control)**, (b) acute **injury**, (c) chronic **injury** experimental time courses. Boxplots represent the 0.05, 0.25, 0.75, 0.95 quantiles of the experimental data. Dark and light grey area plots represent the [0.25, 0.75] and the [0.25, 0.75] quantiles of the posterior predictive distributions, respectively. The green line indicates the posterior mean; the red line, partially overlapping the green line, represents the posterior median. (d)-(e)-(f) Plots representing the posterior predictive distribution of the migration term $\gamma(C - C^*)H(C - C^*)$ in the ileum obtained from control (BrdU) (d), acute **injury** (e) and chronic **injury** (f) time courses. The contribution to migration is reduced during chronic **injury**.

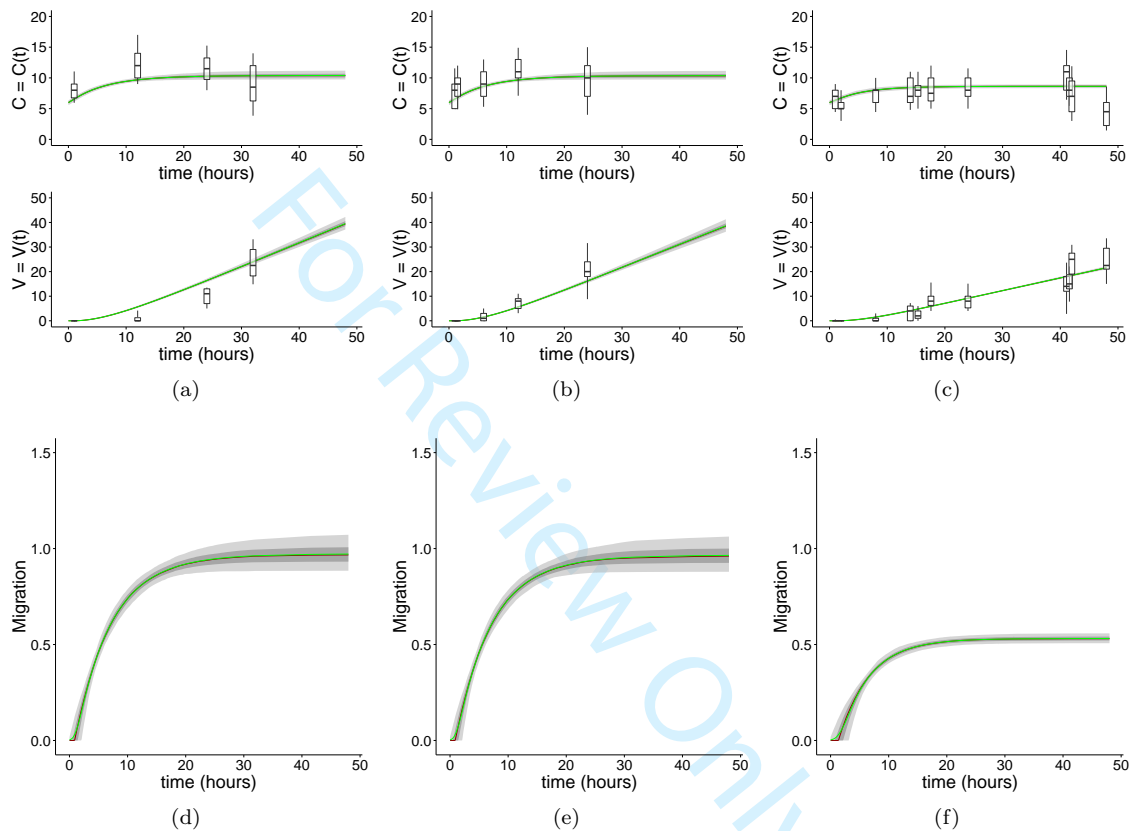


Figure 4: **Fits of the two-compartment model to duodenal time course data.** (a)-(b)-(c) Posterior predictive distributions and estimates of parameter uncertainty obtained by fitting the two-compartment model (Eqs. (1)) against duodenal time courses. Posterior predictive distributions inferred from (a) **BrdU (control)**, (b) acute **injury**, (c) chronic **injury** experimental time courses. Boxplots represent the 0.05, 0.25, 0.75, 0.95 quantiles of the experimental data. Dark and light grey area plots represent the [0.25, 0.75] and the [0.25, 0.75] quantiles of the posterior predictive distributions, respectively. The green line indicates the posterior mean; the red line, partially overlapping the green line, represents the posterior median. (d)-(e)-(f) Plots representing the posterior predictive distribution of the migration term $\gamma(C - C^*)H(C - C^*)$ in the duodenum obtained from control (BrdU) (d), acute **injury** (e) and chronic **injury** (f) time courses. The contribution to migration is reduced during chronic **injury**.

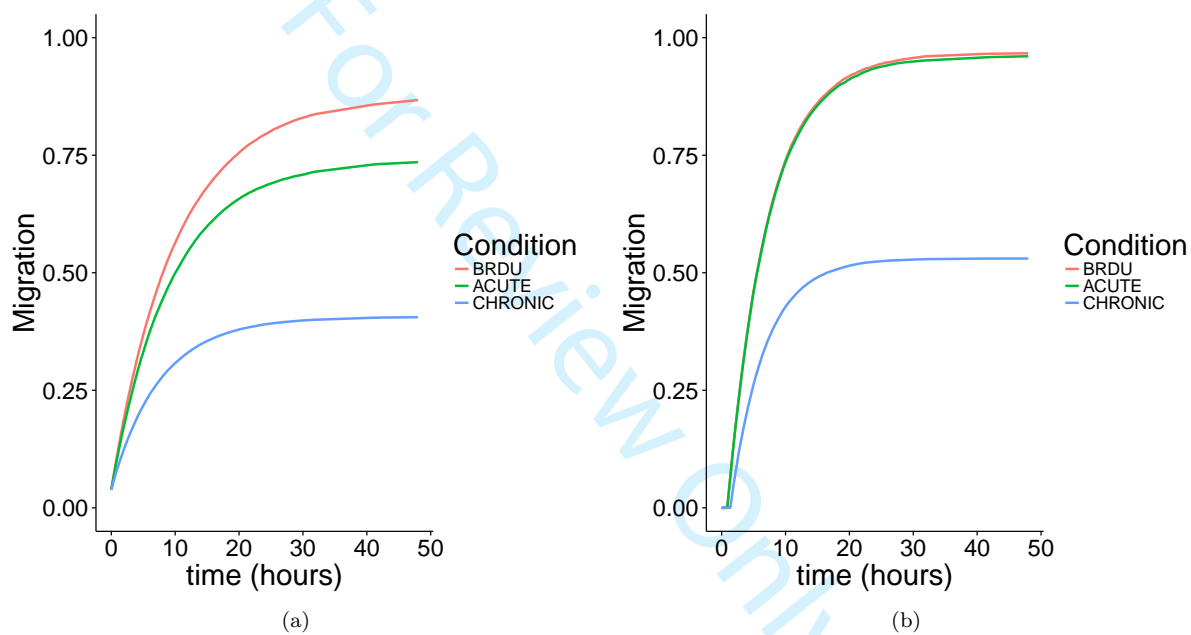


Figure 5: **Migration terms of the two-compartment model when fitted against experimental time courses.** Plots representing the medians of the posterior predictive distribution of the migration terms $\gamma(C - C^*)H(C - C^*)$ in ileum (a) and in duodenum (b). Contribution to migration is reduced during simulated chronic **injury**.

Main Tables

Table 1: Summary of the parameters and initial conditions that appear in the two-compartment model defined by Equations (2).

Parameter	Description	Units
λ	Proliferation rate	h^{-1}
γ	Migration rate into the villus	h^{-1}
μ_{c_a}	Death rate in the crypt during acute injury	h^{-1}
μ_{v_a}	Death rate in the villus during acute injury	h^{-1}
μ_{c_c}	Death rate in the crypt during chronic injury	h^{-1}
μ_{v_c}	Death rate in the villus during chronic injury	h^{-1}
C^*	Number of labelled cells in the crypt above which migration to the villus starts	-
$C_0 \equiv C(t=0)$	Initial number of labelled cells in crypt	-
$V_0 \equiv V(t=0)$	Initial number of labelled cells on villus	-

Table 2: Summary of the parameters and initial conditions that appear in the three-compartment model defined by Equations (3).

Parameter	Description	Units
λ	Proliferation rate	h^{-1}
γ_c	Migration rate from proliferative to non-proliferative state	h^{-1}
γ_v	Migration rate into the villus	h^{-1}
γ_s	Cell shedding rate	h^{-1}
μ_{c_a}	Death rate in the crypt during acute injury	h^{-1}
μ_{v_a}	Death rate in the villus during acute injury	h^{-1}
μ_{c_c}	Death rate in the crypt during chronic injury	h^{-1}
μ_{v_c}	Death rate in the villus during chronic injury	h^{-1}
P^*	Number of proliferative and labelled cells in the crypt above which migration to non-proliferative state starts	-
Q^*	Number of non-proliferative and labelled cells in the crypt above which migration to the villus starts	-
V^*	Number of labelled cells in the villus above which cell shedding starts	-
$P_0 \equiv P(t=0)$	Initial number of labelled proliferative cells in crypt	-
$Q_0 \equiv Q(t=0)$	Initial number of labelled non-proliferative cells in crypt	-
$V_0 \equiv V(t=0)$	Number of labelled cells in villus (all non-proliferative)	-